J Geod (2012) 86:319–335
DOI 10.1007/s00190-011-0521-8

ORIGINAL ARTICLE

Simulation study of a follow-on gravity mission to GRACE

Bryant D. Loomis · R. S. Nerem · S. B. Luthcke

Received: 22 November 2010 / Accepted: 8 October 2011 / Published online: 28 October 2011

Abstract The gravity recovery and climate experiment (GRACE) has been providing monthly estimates of the Earth's time-variable gravity field since its launch in March 2002. The GRACE gravity estimates are used to study temporal mass variations on global and regional scales, which are largely caused by a redistribution of water mass in the Earth system. The accuracy of the GRACE gravity fields are primarily limited by the satellite-to-satellite range-rate measurement noise, accelerometer errors, attitude errors, orbit errors, and temporal aliasing caused by un-modeled high-frequency variations in the gravity signal. Recent work by Ball Aerospace & Technologies Corp., Boulder, CO has resulted in the successful development of an interferometric laser ranging system to specifically address the limitations of the K-band microwave ranging system that provides the satellite-to-satellite measurements for the GRACE mission. Full numerical simulations are performed for several possible configurations of a GRACE Follow-On (GFO) mission to determine if a future satellite gravity recovery mission equipped with a laser ranging system will provide better estimates of time-variable gravity, thus benefiting many areas of Earth systems research. The laser ranging system improves the range-rate measurement precision to ∼0.6 nm/s as compared to ∼0.2 μm/s for the GRACE K-band microwave ranging instrument. Four different mission scenarios are simulated to investigate the effect of the better instrument at two different altitudes. The first pair of simulated missions is flown at GRACE altitude (∼480 km) assuming on-board accelerometers with the same noise characteristics as those currently used for GRACE. The second pair of missions is flown at an altitude of ∼250 km which requires a drag-free system to prevent satellite re-entry. In addition to allowing a lower satellite altitude, the drag-free system also reduces the errors associated with the accelerometer. All simulated mission scenarios assume a two satellite co-orbiting pair similar to GRACE in a near-polar, near-circular orbit. A method for local time variable gravity recovery through mass concentration blocks (mascons) is used to form simulated gravity estimates for Greenland and the Amazon region for three GFO configurations and GRACE. Simulation results show that the increased precision of the laser does not improve gravity estimation when flown with on-board accelerometers at the same altitude and spacecraft separation as GRACE, even when time-varying background models are not included. This study also shows that only modest improvement is realized for the best-case scenario (laser, low-altitude, drag-free) as compared to GRACE due to temporal aliasing errors. These errors are caused by high-frequency variations in the hydrology signal and imperfections in the atmospheric, oceanographic, and tidal models which are used to remove unwanted signal. This work concludes that applying the updated technologies alone will not immediately advance the accuracy

This work was supported by NASA Headquarters under the Earth System Science Fellowship Grant NGT5.

B. D. Loomis
University of Colorado at Boulder, Boulder, USA

Present Address:
B. D. Loomis (✉)
SGT Inc., Greenbelt, MD, USA
e-mail: bloomis@sgt-inc.com

R. S. Nerem
Colorado Center for Astrodynamics Research,
University of Colorado at Boulder, 431 UCB,
Boulder, CO 80309, USA

S. B. Luthcke
Planetary Geodynamics Laboratory, NASA Goddard Space
Flight Center, Code 698, Greenbelt, MD 20771, USA

of the gravity estimates. If the scientific objectives of a GFO mission require more accurate gravity estimates, then future work should focus on improvements in the geophysical models, and ways in which the mission design or data processing could reduce the effects of temporal aliasing.

Keywords GRACE · Time-variable gravity · Mass transport · Satellite gravimetry

1 Introduction

The gravity recovery and climate experiment (GRACE) mission is capable of accurately measuring the gravitational field of the Earth at monthly intervals to a half-wavelength spatial resolution of ∼400 km at the equator. The mission, which was launched in March 2002, consists of two identical satellites orbiting at ∼480 km altitude at an inclination of ∼89°. The two satellites are separated by ∼220 km in the along-track direction. The K-band microwave ranging system provides the dual range and range-rate measurements between the satellites while the global positioning system (GPS) receivers on each satellite allow for precise orbit determination and time-tagging of the satellite-to-satellite range measurements. Each GRACE satellite is equipped with a pair of star trackers for attitude determination and a high precision accelerometer which measures the sum of all non-conservative forces (Tapley et al. 2004). The mission was originally designed for a lifespan of 5 years, but more recent estimates expect that the mission could remain operational until 2013.

The temporal variations in the gravity field measured by GRACE are the result of the redistribution of mass in the Earth system. The GRACE data have made significant contributions to many areas of scientific research including hydrology, oceanography, glaciology, solid Earth science, and geodesy. (A concise summary of GRACE applications is given by Rummel (2003)). The unique global dataset provided by GRACE has led to a strong desire within the scientific community for a new dedicated gravity recovery mission to follow the current mission.

A GRACE Follow-On (GFO) mission would have tremendous benefits for the scientific community. In addition to extending the time-series of data, currently being provided by GRACE, a follow-on mission may be able to determine the Earth's gravity field with an improved spatial and/or temporal resolution. The desire for an improved spatial resolution would likely drive the design of a follow-on mission as this would enable the geographic isolation of important geophysical processes which are currently indistinguishable with the GRACE gravity solutions.

2 An improved gravity mission

The accuracy of the GRACE gravity estimates is primarily limited by the following factors:

- *Satellite-to-satellite measurement precision* This is the primary measurement used to determine the gravity field and the precision of the GRACE system is limited by the K-band wavelength ($\lambda \sim 1.2$ cm).
- *Accelerometer errors* Imperfect removal of the non-conservative forces acting on each satellite corrupts the gravity estimates.
- *Satellite altitude* The gravitational signal attenuates with distance so observing the anomalies in the gravity field at the highest spatial frequencies might require a reduction in satellite altitude.
- *Attitude determination errors* Attitude information is needed to orient the accelerometer measurements and to calculate a geometric correction to the satellite-to-satellite ranging measurements.
- *Background model error and temporal aliasing* As a part of the estimation procedure, the time-variable gravity signals caused by the ocean and solid Earth tides, the atmosphere, and the non-tidal oceanographic mass variations are forward modeled. This isolates the desired signal (e.g. hydrology) from the modeled processes, and reduces the temporal aliasing errors caused by the high-frequency changes in the gravity field which are under-sampled by the monthly GRACE solutions. Temporal aliasing is the result of both the imperfections in the force models and the high-frequency nature of the hydrology signal that GRACE seeks to measure (Thompson et al. 2004).

Improved technologies could reduce the satellite-to-satellite measurement errors, the accelerometer errors, and allow a reduction in the satellite altitude, and these potential improvements are considered in this investigation. Better star trackers could reduce the attitude errors but this error source is not investigated in this study. van Dam et al. (2008) concluded that the problem of temporal aliasing will limit the performance of a GFO once the instrumentation errors are sufficiently reduced. Some recent ideas and proposed GFO designs seek to reduce the issue of temporal aliasing by flying multiple GRACE-like missions simultaneously. This is not a likely scenario for the near future due to the high cost associated with such a mission. Improvements in the accuracy of the force models is a separate issue from the design of a GFO mission, though it is possible that GRACE or GFO data could be used to improve the models. Previous work has already contributed to the design of a potential future satellite gravity recovery mission and a brief summary is given here. A more thorough discussion of the mission design variables

available for a dedicated gravity mission is given by Rummel (2003).

Some suggestions for a GFO mission were made by Bender et al. (2003). Of primary interest to this investigation is the possible use of laser heterodyne measurements between the two orbiting spacecraft, as opposed to the K-band microwave ranging system employed by GRACE. Because a laser ranging device could measure the range and range-rate between the spacecraft with better precision, a GFO mission equipped with such a device should recover the Earth's gravity field with a greater spatial resolution. A simulation study by Sneeuw et al. (2005) showed the dramatic improvements a laser ranging system would provide in recovering the static global gravity field for a variety of low-low satellite-to-satellite configurations.

Bender et al. (2003) and Rummel (2003) also discuss the possibility of flying a GFO mission with a drag-free system [also referred to as the gravitational reference sensor (GRS) in this work]. This is accomplished by isolating a proof mass within the satellite from the surrounding environment, separating it from the non-conservative forces acting on the satellite. A micro-thruster system would then be used to maintain the position of the satellite with respect to the proof mass so that the satellite orbit would not be affected by drag. This would eliminate the need to include the accelerometer data in the data processing and should remove the correlated acceleration errors that corrupt the GRACE gravity estimates. A drag-free system would also allow a GFO mission to be flown at a lower altitude than would otherwise be possible, since the increased drag forcing at lower altitudes would cause the orbit to decay rapidly if not consistently counteracted with thrusting. It is of course advantageous to fly a follow-on mission in as low an altitude as possible since the gravity signal attenuates with distance. The mission altitude is constrained by the amount of thrusting required to maintain the desired orbit in the presence of the increased non-conservative forces at lower altitudes.

A detailed investigation into the feasibility of a drag-free follow-on mission is performed by Marchetti et al. (2008). The work shows that assuming 87 kg of propellant mass, a GFO mission would have a lifetime of 0.76 years for an orbital altitude of 160 km and 2.27 years for an altitude of 225 km. To extend the 225 km altitude case to 5 years would require approximately 170 kg.

A GFO mission consisting of a four satellite cartwheel formation was first proposed by Bender et al. (2003), and the performance of several formation flying gravity missions are investigated by Sneeuw et al. (2005). In a study by Wiese et al. (2008), four different GFO satellite configurations are considered: a two-satellite co-orbiting pair similar to GRACE, a four-satellite configuration with two co-orbiting pairs, a two-satellite cartwheel formation, and a four-satellite cartwheel formation. The results show that for a case where only the satellite-to-satellite ranging noise is considered, the cartwheel cases perform about an order of magnitude better than the co-orbiting cases and drastically reduce the striping in the spatial error maps. However, when errors due to the mismodelling of the time-variable signal in the atmosphere and oceans are included, the cartwheel orbits perform slightly worse than the co-orbiting cases at high spatial frequencies.

This study is in conjunction with the development of an interferometric laser ranging system by Ball Aerospace & Technologies Corp., Boulder, CO. Completing in December 2006, the project resulted in the successful development of a laser ranging device for use on a GFO mission. Details are presented in Dehne et al. (2009), Nerem et al. (2006), and Pierce et al. (2008). In summary, the new instrument will improve the range-rate precision from $\sim$0.2 μm/s to $\sim$0.6 nm/s.

Multiple GFO configurations are considered in this simulation study to determine the effect of the different designs on mission performance. The variables for the simulated missions are the level of satellite-to-satellite range-rate measurement noise, the method of removal of non-conservative forces, and the satellite altitude and separation distance. This study investigates the performance of GRACE and three GFO missions. The parameters that define these missions are summarized in Table 1.

The GFO Case 3 is the best-case simulated scenario as it provides the most precise range-rate measurements, more effectively removes the non-conservative forces acting on the satellites, and reduces the satellite altitude. GFO Case 1 and GFO Case 2 represent hybrid missions where each is equipped with one, but not both of the improved technologies. The details that define these different missions are presented in the following section.

3 Simulation models and procedure

Numerical simulations are performed to assess the performance of the various GFO missions. The simulation procedure is summarized by three steps: (1) generate simulated satellite-to satellite range-rate data and satellite position data, (2) estimate satellite state initial conditions and empirical

Table 1 Summary of gravity mission configurations

Mission	Altitude / satellite sep (km)	Sat-to-sat range-rate noise	Removal of non-conserv forces
GRACE	480/220	K-band	Accelerometer
GFO #1	480/220	Laser	Accelerometer
GFO #2	250/50	K-band	Drag-free
GFO #3	250/50	Laser	Drag-free

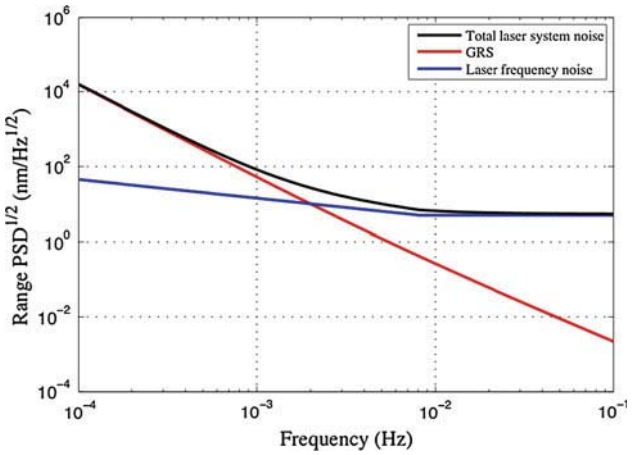

Fig. 1 Spectral density for interferometric laser ranging system errors with 50 km spacecraft separation (not all individual error components are shown)

satellite accelerations, and (3) estimate the gravity field and adjust the satellite state. All numerical simulations are performed using the GEODYN orbit determination software and SOLVE large linear systems solver which were provided by the NASA Goddard Space Flight Center.

3.1 Measurement errors

The inter-satellite range-rate measurements are the primary data type for GRACE and the instrument precision directly relates to the spatial resolution of the solutions. The K-band microwave ranging system employed by GRACE is approximated by a white noise spectral density of 1.8 μm/$\sqrt{\text{Hz}}$ in terms of range. A detailed term-by-term error budget spectral density for the laser ranging system is presented by Pierce et al. (2008). The spectral density of the total laser ranging system error for a 50 km spacecraft separation is shown in Fig. 1 along with the two largest components of the error. The laser frequency noise is the dominant error at the higher frequencies and its power is correlated with the spacecraft separation distance. The GRS error describes the effect of drag-free operation on the precision of the laser ranging measurements and dominates at low frequencies. The segregated GRS error is needed to simulate the noise characteristics for GFO Case 2.

Both error budgets, given in terms of range, are converted to a spectrum of errors in terms of range-rate. This power spectrum is then converted to a time-series of range-rate errors by randomizing the phase of the discretized power spectrum amplitudes and taking the inverse fast Fourier transform (IFFT) over the frequency band 10^{-4} to 10^{-1} Hz. This results in a RMS range-rate error of $\sim$0.21 μm/s for the K-band system and $\sim$0.58 nm/s for the laser.

Table 2 Spectral density of accelerometer errors for satellite axes (frequency band of 10^{-4} to 10^{-1} Hz)

Direction	PSD$^{1/2}$
Radial	$(1+0.005/f)^{1/2}\times 10^{-10}$ m/s^2/Hz$^{1/2}$
Transverse	$(1+0.005/f)^{1/2}\times 10^{-10}$ m/s^2/Hz$^{1/2}$
Normal	$(1+0.1/f)^{1/2}\times 10^{-9}$ m/s^2/Hz$^{1/2}$

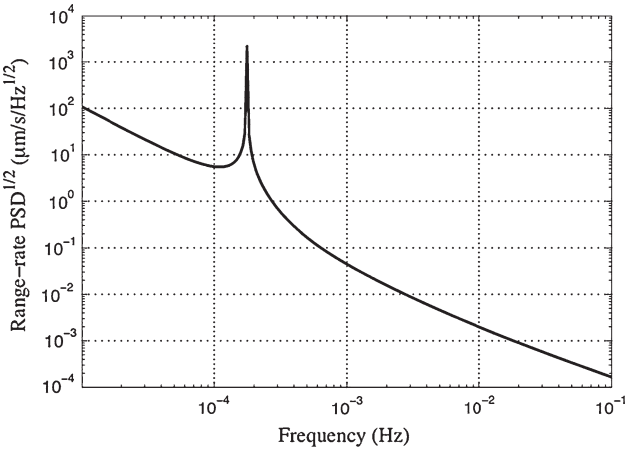

Fig. 2 Spectral density of satellite-to-satellite range-rate error due to accelerometer error

Each of the GRACE satellites is equipped with an accelerometer that measures the electrostatic force required to hold the position of a center-of-gravity proof mass constant with respect to the satellite. The accelerometer data are then used to differentiate between the gravitational and non-gravitational forces that act on each satellite. The procedure for including the GRACE accelerometer errors used in this study is developed by Kim (2000) and applies a transfer function between the perturbed satellite motion and the range-rate measurement. Table 2 gives the spectral density of the accelerometer errors for the radial, transverse, and normal satellite directions and Fig. 2 shows the corresponding effect on the satellite-to-satellite range-rate. The IFFT is then applied to this spectral density to generate the time-series of range-rate errors that results from the accelerometry which must be included in the GRACE and GFO Case 1 simulations. The large spike in Fig. 2 corresponds to the one cycle-per-revolution frequency for GRACE.

The effect that the accelerometer errors have on the gravity solutions is mitigated by estimating a set of empirical satellite accelerations (this procedure is further discussed in Sect. 3.5). The reduction in range-rate errors from the removal of empirical parameters is simulated here by estimating a constant and one cycle-per-revolution amplitude and phase for a 1-day arc time-series containing the sum of the accelerometer and inter-satellite sensor errors (only GRACE and GFO Case 1). The resulting range-rate error spectral densities for

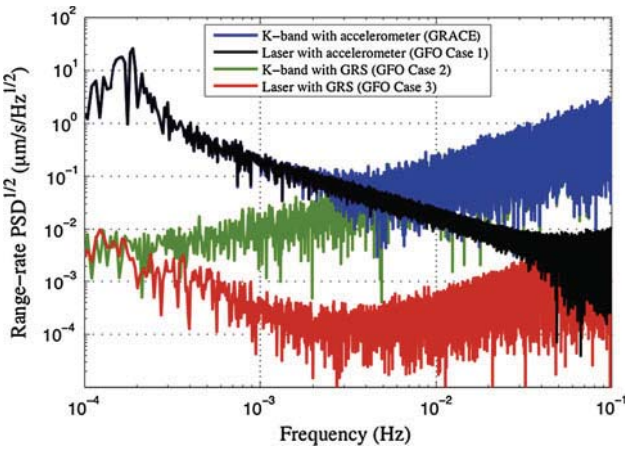

Fig. 3 Spectral densities of range-rate errors for each simulated mission scenario computed with a 1-day arc (after the estimation of empirical parameters for GRACE and GFO Case 1)

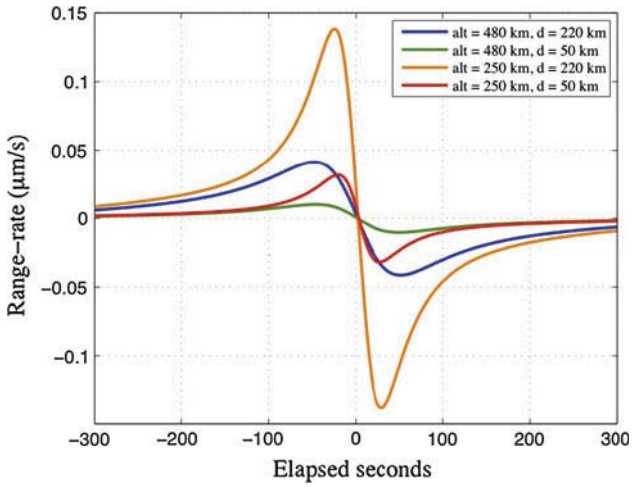

Fig. 4 Satellite-to-satellite range-rate observations for a direct flyover of a 1° × 1° block with 100 cm water mass for different altitudes (480 and 250 km) and spacecraft separations distances (220 and 50 km). The *blue line* describes the GRACE and GFO Case 1 missions and the *red line* describes the GFO Case 2 and GFO Case 3 missions

the four simulation cases are provided in Fig. 3. The accelerometer errors clearly dominate at the lower frequencies for GRACE and GFO Case 1, and their spectra diverge at the point the K-band ranging errors become larger than the accelerometer errors. It is also interesting to note that the range-rate error spectrum of GFO Case 1 only approaches that of GFO Case 3 for the highest frequencies, while GFO Case 3 is significantly lower than GFO Case 2 everywhere except at the very lowest frequencies.

The gravity estimation procedure requires that the satellite orbits are accurately determined. For GRACE, the orbits are usually determined using a reduced dynamic orbit determination method which combines GPS tracking data with orbital dynamics (Bertiger et al. 2002). The effect of the GPS tracking errors is introduced into the simulations by adding a Gaussian white noise with $\sigma = 1.0$ cm to the simulated truth position vectors in all three axis directions. This approximates the precision of GRACE orbit determination shown by Kang et al. (2006).

3.2 Orbital parameters

The selection of the orbital parameters will be a key part of the GFO mission design as it affects mission performance. It is assumed here that a GFO mission will be placed in a near-polar, near-circular orbit as with GRACE, since these conditions are needed to provide global coverage. As previously discussed, the selection of the orbital altitude is of great importance, as lower altitude satellites are more sensitive to the higher spatial resolution features in the gravity field. The desire to fly a lower altitude satellite will need to be weighed against the mission lifetime as the increase in the forcing from atmospheric drag increases the required thrust capabilities to maintain the orbit or implement a drag-free system. The spacecraft separation distance is also a key mission design parameter as the separation distance affects the level of instrument noise and the ability of the mission to recover the gravity signal at various wavelengths (Sneeuw et al. 2005). Lastly, the ground track of the mission must provide consistent global coverage since this is needed to generate global gravity estimates. It is also important to avoid resonant orbit periods as this degrades the gravity solutions.

The important gravity mission design considerations associated with the orbital altitude and spacecraft separation are illustrated in Fig. 4, which plots the satellite-to-satellite range-rate signal for the four possible mission configurations defined by two mission altitudes (480 and 250 km) and two spacecraft separation distances (220 and 50 km), for a direct flyover of a 1° × 1° block with 100 cm water mass.

Comparing missions with the same spacecraft separation and different altitudes clearly shows that reducing the altitude increases the magnitude of the signal. Comparing the different spacecraft separation values reveals that decreasing this distance has the combined effect of dramatically reducing the signal strength while increasing the signal frequency. To have a range-rate signal strength similar to GRACE, with a spacecraft separation of 50 km (to achieve the level of instrument precision described by Fig. 1), requires that the altitude be reduced to ∼250 km. This work applies these aforementioned configurations, where the GRACE satellites have an altitude of 480 km and a separation distance of 220 km, and a possible GFO configuration has an altitude of 250 km and a separation distance of 50 km.

The increase in signal frequency that results from a shorter spacecraft separation would enable the mission to recover gravity anomalies to a finer spatial resolution, provided they are observable in the presence of the instrument noise.

Table 3 Mission orbital parameters summary

	480 km altitude 220 km separation	250 km altitude 50 km separation
a	6860.813 km	6632.876 km
e	1.36×10^{-4}	1.15×10^{-5}
i	89.015°	89.458°

Table 4 Force models used for numerical simulations

	Truth	Nominal
Static	EIGEN-GL04C	EIGEN-GL04C
Tidal	FES2004	GOT00
Atmospheric	ECMWF	NCEP
Oceanographic	OMCT	MOG2D

Analyzing the plots in Fig. 4 gives a half-period of 100 s for the 480 km/220 km case and a half-period of 47 s for the 220 km/50 km case, which translates to signal frequencies of 5 and 10.6 mHz, respectively. The observation signal frequencies are about the same for the plotted scenarios with common separation distances.

The ground tracks of both orbit configurations provide good global coverage about every 30 days. The largest ground track spacing after 30 days is ∼1° for the 480 km altitude orbit and ∼0.8° for the 250 km altitude orbit. Table 3 summarizes the key orbital elements for the two cases.

3.3 Force models

Several of the geophysical processes which cause temporal variations to the Earth's gravity field are modeled and removed prior to the estimation of the gravity field. These include mass variations caused by the solid Earth and ocean tides, and atmospheric and non-tidal oceanic mass variations. Errors in the models used to remove these signals can cause significant errors in the gravity estimates for GRACE. The inclusion of these background model errors in the simulations is necessary for a realistic assessment of GRACE and GFO mission performance. *Truth* force models are used to simulate truth data and *Nominal* force models are used for the gravity estimation. The difference between the models is then considered the level of uncertainty for each geophysical process. This procedure, which assumes that the differences between two different geophysical models represents the error of that model, has been a common practice for GRACE simulation studies. In addition to the direct effect the background model errors have on the solution, the time-variable nature of the errors causes temporal aliasing (Han et al. 2004; Seo et al. 2008; Seo and Wilson 2005; Thompson et al. 2004). A table summarizing the force models used in the simulations is given in Table 4.

Since the focus of this study is the recovery of the time-variable gravity signal, errors in the static gravity field are neglected using the same *Truth* and *Nominal* model.

The *Truth* tidal model is the finite element solution (FES) model which is computed using the tidal hydrodynamic equations assimilated with tide gauge and TOPEX/Poseidon data (Lefèvre et al. 2002). The *Nominal* tidal model is the Goddard Ocean Tide (GOT) model which is an assimilated model computed from years of the TOPEX/Poseidon data (Ray 1999). The respective *Truth* and *Nominal* atmospheric models are the European Centre for Medium Range Weather Forecasts (ECMWF) and the National Centers for Environmental Prediction (NCEP) models which are both formed using a global network of meteorological stations. To model the oceanographic signal the ocean model for circulation and tides (OMCT) and MOG2D (2D Gravity Waves model) models are used for the *Truth* and *Nominal* respectively.

The atmospheric and oceanographic models are added and input into GEODYN as 3-hourly sets of spherical harmonics (the sum of these models is commonly referred to as the atmosphere and ocean de-aliasing (AOD) product). The sum of ECMWF and OMCT is directly available as the GRACE AOD1B (AOD level-1b) product from <ftp://podaac.jpl.nasa.gov/grace/>. It should be noted that the atmospheric tides are present in the ECMWF/ OMCT model but are not present in the NCEP/ MOG2D model. For this reason the atmospheric tides are removed from the FES2004 tidal model but not from the GOT00 model.

To effectively determine the ability of a GFO mission to recover the gravity field, it is necessary to estimate the time-variable gravity signal at multiple locations on the Earth's surface. In this study, gravity estimates are simulated for Greenland and the Amazon and surrounding basins of South America. These locations were chosen because of their interest to the scientific community, the differences in groundtrack coverage, and the different level of force model errors for the two regions. Errors in the atmospheric, oceanic, and tidal models have a spatial dependence due to limitations in the availability and quality of the data that is used to form the models. The geographical AOD errors presented in Fig. 5 show that this error source will have a greater effect on time-variable gravity estimates for Greenland than South America.

The *Truth* hydrological signal, which is estimated by the numerical simulations over South America is the global land data assimilation system (GLDAS) hydrology model developed by Rodell et al. (2004). As with the time-varying atmospheric and oceanic signal, the GLDAS *Truth* signal is input into GEODYN as 3-hourly sets of spherical harmonics. The *Truth* GLDAS signal is included up to spherical harmonic degree and order 72 and the *Nominal* set of force models does not contain any hydrological signal.

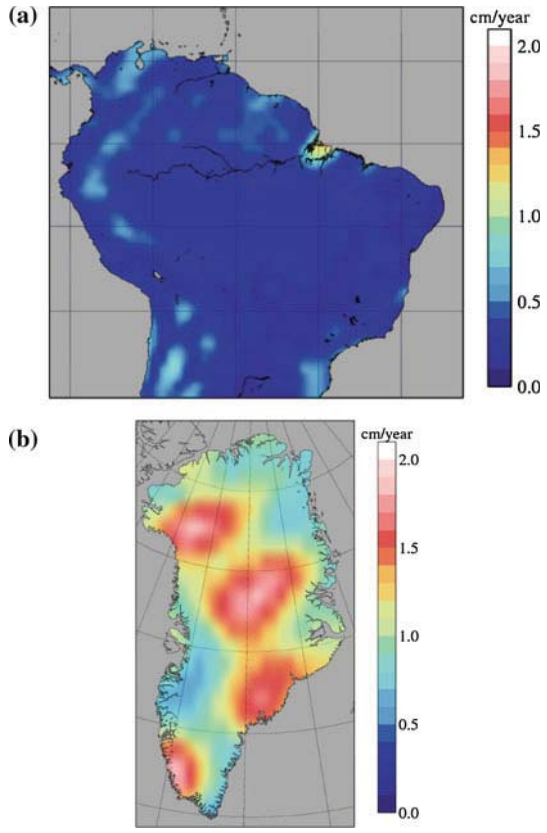

Fig. 5 South America (**a**) and Greenland (**b**) AOD model error RMS about the mean computed with 12 monthly means (ECMWF/OMCT minus NCEP/MOG2D for January 2003–December 2003)

A model for ice mass change over Greenland is not readily available, so a *Truth* model is constructed. The *Truth* model for Greenland is a $1^\circ \times 1^\circ$ grid for which each block is assigned a mass trend and an amplitude of the annual signal where the strength of the annual signal is dependent on the elevation of the block. These monthly *Truth* grids are converted into spherical harmonics prior to being used as input for GEODYN with an expansion to degree and order 180. The mass trend values for the individual $1^\circ \times 1^\circ$ blocks range from +0.2 GT/year to −4.7 GT/year with the largest losses concentrated along the western and south-eastern coasts. The high elevation interior (above 2,000 m) of Greenland has a uniform annual signal amplitude of 50 GT and a total mass trend of −47.1 GT/year while the low-elevation coastal region (below 2,000 m) has a uniform annual amplitude of 300 GT and total trend of −95.2 GT/year. The synthetic *Truth* Greenland ice mass signal has a higher spatial resolution than can be observed by GRACE.

3.4 Temporal aliasing errors

Temporal aliasing errors exist when a measured signal has a higher frequency than half the sample rate (Nyquist frequency). For GRACE, aliasing errors exist because water mass changes from atmospheric, oceanographic, tidal, and hydrologic signals occur at time scales of a few hours, while GRACE gravity solutions are usually formed about once per month (Wahr et al. 2004). A number of studies have shown that the problem of temporal aliasing is a major source of error for GRACE (Han et al. 2004; Thompson et al. 2004). This error is introduced into the simulations for both locations using a different set of *Truth* and *Nominal* models with a high temporal frequency as explained above. The non-uniform character of the model errors illustrated by Fig. 5 causes the temporal aliasing errors to be dependent on geographic location and the satellite groundtrack. Additional temporal aliasing errors occur for the South America simulations due to the high frequency of the GLDAS *Truth* signal to be estimated (the synthetic *Truth* signal for Greenland ice mass changes does not vary at sub-monthly time scales).

3.5 Gravity recovery simulation procedure

The simulation procedure is summarized by three steps:

Step 1. *Truth* satellite-to-satellite range-rate data and satellite ephemeris are generated by propagating the satellites with the *Truth* set of force models and initial conditions as input. Mission specific range-rate measurement noise and accelerometer noise is added to the *Truth* range-rate data. Errors are also added to the satellite ephemeris data. The noisy data are representative of the data which would be available from a real GRACE or GFO mission.

Step 2. Satellite initial conditions and empirical satellite accelerations are estimated with the *Nominal* set of force models and the noisy range-rate and satellite position data from *Step 1*.

Step 3. The observation residuals and partial derivatives are computed with the *Nominal* set of force models, the noisy range-rate data, the estimated satellite initial conditions from *Step 2*, and the estimated empirical satellite accelerations from *Step 2*.

The gravity solutions are formed by estimating a series of mass concentration blocks (mascons), which uses a set of differential potential coefficients to represent a small uniform layer of mass over a region (Luthcke et al. 2008). The regional mascon estimation method provides large benefits in reducing computation time as compared to forming global gravity estimates, especially when estimating the gravity field to a high spatial resolution as is done in this study, where each mascon is a $1^\circ \times 1^\circ$ block described by a spherical harmonic expansion to degree and order 180. The estimated mascons are spatially constrained and the relative weighting between the data and constraint matrices is determined by the quality

of the data. Increasing the weight applied to the constraint matrices effectively reduces the spatial resolution of the estimates.

Rowlands et al. (2010) showed that estimating a global set of mascons, without additional geolocatable physical constraints, results in solutions with comparable accuracy as a spherical harmonic solution with approximately the same number of parameters. However, Rowlands et al. (2010) also observed that the addition of appropriate geolocatable constraints does lead to improvements in solution accuracy, and this approach is applied here. In this study, separate constraint matrices are written for the land and ocean mascons, forcing the signals for these mascons to be uncorrelated. An additional constraint is applied to the Greenland solutions, such that only land mascons in the same elevation range (above or below 2,000 m) are constrained to each other. A similar procedure for constraining Greenland mascons by elevation was applied by Luthcke et al. (2006).

A set of empirical satellite accelerations are estimated in *Step 2* of the simulation procedure to mitigate the effect of the accelerometer errors. The selected parameters and the frequency of their estimation were tuned to most accurately recover the gravity field in the presence of the accelerometer errors. The best-case procedure estimates a constant and one cycle-per-revolution terms in the along track direction at 3-h intervals, and one cycle-per-revolution terms in the radial and normal directions and a constant in the normal direction once per 24-h arc.

3.6 Simulation scenarios

Three different simulations are performed in this study. The first simulation investigates the ability of each mission to recover a 1° × 1° static block of mass at the equator with 31 days of data. For this case, only the measurement errors discussed in Sect. 3.1 are included. Since the force model errors are not included, and the estimated signal does not vary with time, no temporal aliasing errors are present in this scenario. The results of this simulation reveal the spatial resolution limits imposed by the instrumentation errors of each mission.

Next, 25 months (January 2003–January 2005) of time-variable gravity signals in South America and Greenland are estimated. Once again the measurement errors are included in this scenario while the errors in the force models are not. (It is important to note that temporal aliasing errors are still present in the South America solutions due to the high-frequency nature of the *Truth* GLDAS hydrology signal which is estimated by the simulation.)

The final simulation estimates the same time-variable gravity signals for the 25-month span where both the measurement errors and the force model errors are included. This final simulation scenario is the most realistic, so should be most indicative of performance for the various missions given the assumed accuracy of the force models.

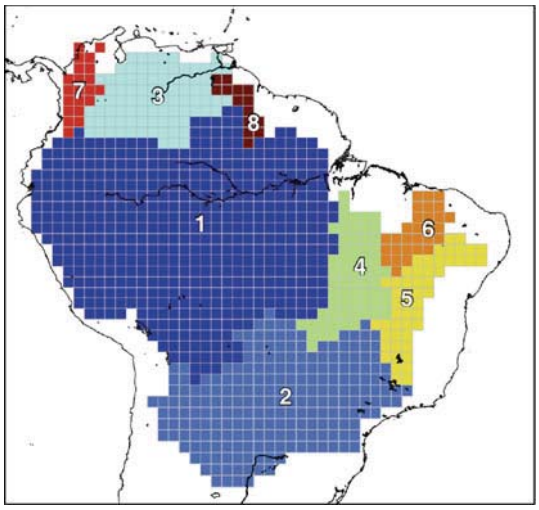

Basin #	Surface Area ($10^5 km^2$)	No. of mascons
1	60.856	497
2	25.516	223
3	10.720	87
4	7.7670	64
5	6.1403	51
6	3.5660	29
7	2.5826	21
8	1.7273	14

Fig. 6 South America basin definitions

The same set of 1° × 1° mascons is estimated for all three simulation scenarios. The solutions and the methods used to analyze their accuracy are discussed in Sect. 4.

3.7 Basin definitions

GRACE data are commonly used to determine a time-series of mass variations within a particular region or drainage basin. To analyze the results of the simulations in the same way, a set of basins are defined for both South America and Greenland and are shown in Figs. 6 and 7, respectively.

4 Results

4.1 Static block of mass: measurement errors only

The results presented here show the ability of each gravity mission to recover a small static block of mass. A set of local mascons is estimated using 31 days of simulated data where the *Truth* signal is 100 cm of water over a 1° × 1° block at the equator in the Amazon basin and only the measurement errors discussed in Sect. 3.1 (range-rate, accelerometer, and

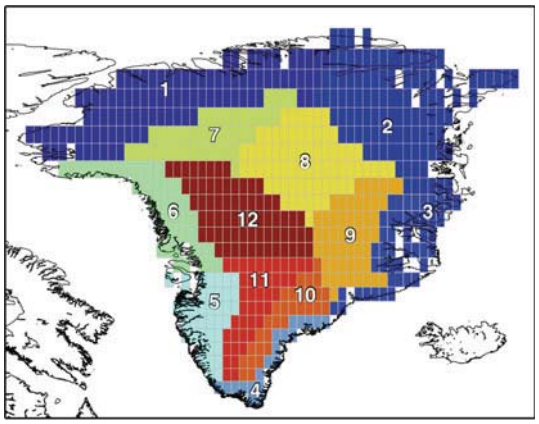

Basin #	Surface Area ($10^5 km^2$)	No. of mascons
1	2.0752	99
2	2.2534	104
3	1.7889	46
4	1.0992	20
5	1.9494	40
6	1.4956	44
7	1.0332	42
8	1.9097	68
9	1.9137	51
10	1.4674	30
11	1.9638	42
12	2.3570	68

Fig. 7 Greenland basin definitions

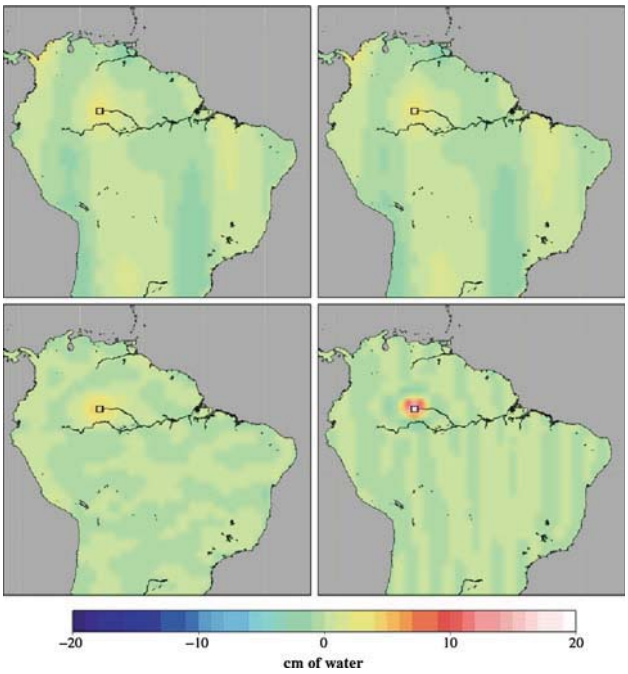

Fig. 8 Gravity estimates for 1° × 1° block of 100 cm of water for different mission configurations: GRACE (*top-left*), GFO Case 1 (*top-right*), GFO Case 2 (*bottom-left*), and GFO Case 3 (*bottom-right*). The location of the *Truth* signal is shown on each plot

satellite state) are included. The simulation results in this section aim to investigate the best attainable spatial resolution of the gravity estimates for each mission. As discussed earlier, the errors caused by temporal aliasing are largely dependent on location, so it is not practical to discuss the spatial resolution of a mission for global gravity estimation in the presence of temporal aliasing errors.

The spatial plots of the gravity estimates for all simulated missions are shown in Fig. 8. Comparing the results of GFO Case 2 and 3 shows a clear improvement in recovering the block of mass with the laser ranging system for the low-altitude drag-free case. The high-altitude accelerometer cases (GRACE and GFO Case 1), however, are indistinguishable. Though the GRACE and GFO Case 1 gravity field estimates correctly locate the high signal over the 1° × 1° block at the equator, there are other locations where the estimated signal deviates significantly from the *Truth*. These errors are characterized by large North–South stripes that result from the mid-to-low frequency accelerometer errors which have a different spatiotemporal realization for each of the many ground tracks that pass through the considered region. This point is illustrated by the fact that these large-scale striping errors are not present in the drag-free GFO Case 2 solution even though this lower-altitude mission scenario has a slightly smaller observation signal magnitude than GRACE (see Fig. 4). This implies that the improved GFO Case 2 result as compared to GRACE is due to the drag-free system and not the reduced altitude.

A more quantitative comparison of performance is given in Fig. 9. This plot shows the total amount of recovered mass in a series of increasingly larger concentric blocks centered on the location of the *Truth* mass. The table in Fig. 9 provides the box sizes and corresponding surface areas at which the simulated gravity estimates are sampled. The true amount of mass within the block is 12.4 GT and is included in the figure as a point of comparison. GFO Case 3 performs significantly better than the other missions as it measures nearly all of the mass within a 3° × 3° block. This result is expected as this mission has the lowest instrumentation error and has the added benefit of the improved spatial resolution associated with the reduced spacecraft separation. GFO Case 2 performs better than the other two missions by recovering more mass within each of the sampled boxes and close to all of the mass for a 7° × 7° block. The GRACE and GFO Case 1 missions do not recover all of the mass for any size block, which again is due to the accelerometer errors. It is important to note that for a different simulated month, it would be just as likely that GRACE and GFO Case 1 would overestimate the mass within the block, as each month has a different groundtrack and a different error time-series resulting in a unique spatial manifestation of the accelerometer errors.

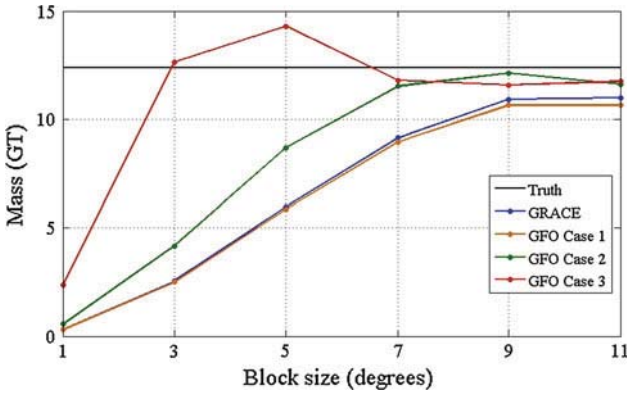

Box size (degrees)	Surface Area (km^2)
$1° \times 1°$	1.239×10^4
$3° \times 3°$	1.115×10^5
$5° \times 5°$	3.096×10^5
$7° \times 7°$	6.068×10^5
$9° \times 9°$	1.002×10^6
$11° \times 11°$	1.497×10^6

Fig. 9 Mass recovered within a given size block for different mission configurations: instrument noise only. Truth value is given by *black line*. Table shows the surface area of each block size

4.2 Time-variable gravity: measurement errors only

This section presents simulated solutions of the time-variable gravity signal where the measurement errors are included (range-rate, accelerometer, and satellite state) and the imperfections in the geophysical models are not. While the results in this section are optimistic, they do provide valuable insight into the effect of the instrument noise on time-variable gravity recovery, and the temporal aliasing problem that exists when measuring the rapidly varying hydrology signal with a single satellite mission. (The simulated *Truth* Greenland ice mass signal does not have a high temporal frequency like the GLDAS hydrology model estimated over South America).

The results of the time-variable gravity simulations are analyzed with two methods. The first analysis method computes the spatial map of the gravity errors by differencing the maps of the *Truth* and estimated gravity fields for each of the simulated 25 months. The spatial RMS error is then computed for each monthly map, and the mean of these values is calculated resulting in the average spatial RMS error for each mission and location. Results of the spatial RMS errors for all time-variable gravity simulations are listed in Table 5.

The second analysis method computes the time-series of mass change within the basins defined by Figs. 6 and 7 by summing the mascons within each basin at each time step. Measuring basin-scale mass changes is a common application for the GRACE gravity solutions. The estimated time-series of mass changes are also used to compute the trend and annual signal within each basin that best fit the data, and the results are compared to the *Truth* values. The South American basin trends and estimated trend differences are not reported as they are not statistically significant for the majority of the basins due to the small trends and relatively short span of data.

Table 5 Mean spatial RMS errors for all time-variable gravity simulations

Mission	Mean spatial RMS error (cm of water)			
	Meas. noise only		All errors	
	S. Amer.	Green.	S. Amer.	Green.
GRACE	3.44	5.42	3.95	6.59
GFO #1	3.44	5.44	3.95	6.59
GFO #2	2.78	3.92	3.81	5.78
GFO #3	2.77	2.81	3.82	5.78

The results of the South America simulations give average spatial RMS errors of 3.44, 3.44, 2.78, and 2.77 cm of water for the GRACE, and GFO Case 1, 2, and 3 missions respectively. These results show that there is essentially no difference between the GRACE and GFO Case 1 mission performance, and the GFO Case 2 and GFO Case 3 mission performance for recovering the time-variable GLDAS hydrology signal over South America for the measurement noise only case. This suggests that the temporal aliasing caused by under-sampling the GLDAS hydrology signal significantly limits the effectiveness of the improved ranging instrument, even for GFO Case 3 which saw an improved solution over GFO Case 2 when estimating a static block of mass. Due to similarities in performance to the other missions, further analysis of the South America results is only done for the GRACE and GFO Case 3 missions.

The mass variations for each South American basin (Fig. 6) computed by the GRACE and GFO Case 3 gravity solutions and the *Truth* GLDAS hydrology signal are shown in Fig. 10. Table 6 gives the *Truth* signal RMS and the RMS of the difference between the *Truth* and the estimate for each mission and each basin. The gravity estimates for GFO Case 3 have a lower error RMS than GRACE for seven of the eight basins with varying levels of improvement for those basins. The *Truth* values for annual amplitude and phase and their errors for each mission are given in Table 7. Not surprisingly, the mission with the lower error RMS from Table 6 also tends to more accurately determine the annual signal. For Greenland the average spatial RMS errors are 5.42, 5.44, 3.92, and 2.81 cm of water for the GRACE, and GFO Case 1, 2, and 3 missions respectively. Once again there is no significant difference in the accuracies of the GRACE and GFO Case 1 missions. However, unlike with the South America simulation, this scenario does show a difference in performance between the GFO Case 2 and GFO Case 3 solutions. The reason the laser provides improvement in this case is

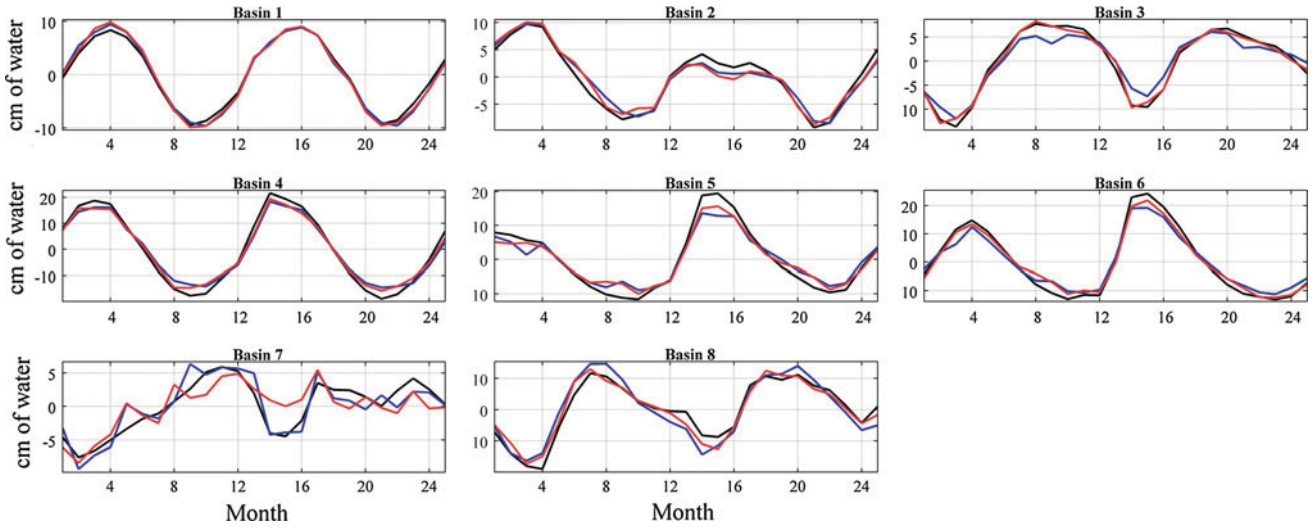

Fig. 10 South America basin mass variations for missions with measurement errors only: Truth (*black*), GRACE (*blue*), and GFO Case 3 (*red*)

Table 6 Statistical analysis of South American basin mass variations: measurement errors only (cf. Fig. 10)

Basin	Truth RMS (cm of water)	Truth−Estimate RMS (cm of water)	
		GRACE	GFO 3
1	6.222	0.748	0.728
2	5.459	1.254	1.229
3	6.705	1.840	0.752
4	13.609	2.552	2.049
5	9.076	2.625	2.138
6	11.844	2.701	1.810
7	3.790	1.682	2.322
8	8.907	3.242	2.164

Table 7 Truth and simulated errors (Truth minus estimate) of best fit annual amplitude and annual phase: South America measurement errors only (cf. Fig. 10)

Basin	Annual amplitude (cm)			Annual phase (°)		
	Truth	Truth−Est.		Truth	Truth−Est.	
		GRACE	GFO 3		GRACE	GFO 3
1	9.21	−0.30	−0.47	10.52	1.02	1.10
2	7.04	1.24	1.27	27.87	4.66	0.57
3	8.40	2.55	0.46	219.58	−0.85	−0.79
4	19.18	3.35	2.80	26.41	4.06	1.00
5	12.48	3.23	2.72	24.33	2.65	4.16
6	15.97	3.39	2.33	2.28	−0.35	3.21
7	3.24	−0.12	2.06	195.61	1.16	−24.34
8	9.69	−2.95	−0.77	236.32	−6.35	−2.70

because the estimated ice mass change signal does not have a high temporal frequency like the hydrology signal, so aliasing does not degrade the gravity solution.

The time-series of mass changes within the Greenland basins (Fig. 7) are computed for the *Truth* model of ice mass change, and for the GRACE, GFO Case 2 and GFO Case 3 mission estimates. The plotted results are shown in Fig. 11 and the corresponding RMS values of the *Truth* signal and the errors for each mission and basin are in Table 8. GFO Case 3 has the lowest RMS values for 9 of the 12 basins with many of the basins showing a dramatic improvement in accuracy for GFO Case 2 and GFO Case 3 as compared to GRACE. The *Truth* and estimated trends for each basin are given in Table 9. The differences between the *Truth* and estimated values of the trend and annual signal are listed in Table10. Accurate determination of the Greenland ice mass trends is of great importance to the scientific community, and these results show that for many of the basins GFO Case 3 provides a significant improvement in determining the trend over GRACE.

4.3 Time-variable gravity: all errors

The results discussed here now include all significant errors sources (measurement noise and force model errors) and are analyzed using the same methods as in the previous section.

For this case, the South America simulations result in average spatial RMS errors of 3.95, 3.95, 3.81, and 3.82 cm of water for the GRACE, and GFO Case 1, 2, and 3 missions, respectively. As was observed for the South America measurement noise only case, there is no difference in accuracy between the GRACE and GFO Case 1 missions or between the GFO Case 2 and GFO Case 3 missions. Once again the mass variations and corresponding statistics are computed

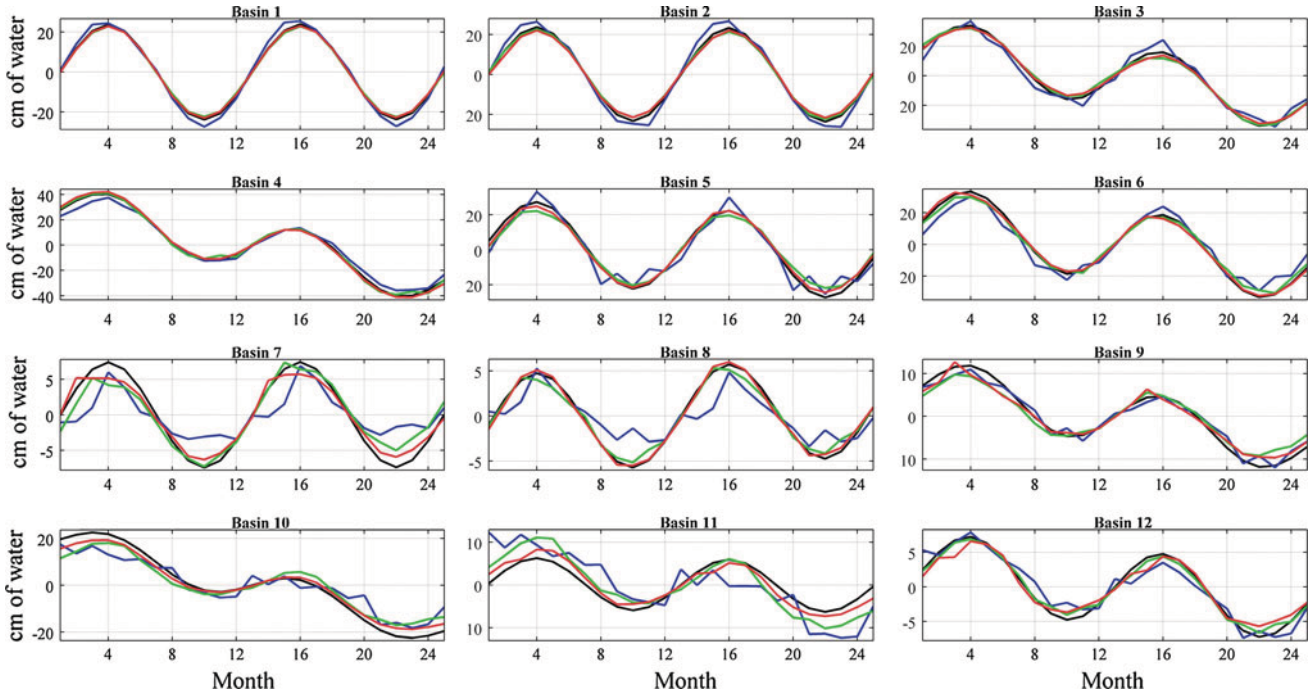

Fig. 11 Greenland basin mass variations for missions with measurement errors only: Truth (*black*), GRACE (*blue*), GFO Case 2 (*green*), and GFO Case 3 (*red*)

Table 8 Statistical analysis of Greenland basin mass variations: measurement errors only (cf. Fig. 11)

Basin	Truth RMS (cm of water)	Truth−Estimate RMS (cm of water)		
		GRACE	GFO 2	GFO 3
1	16.513	2.087	0.793	0.592
2	16.306	2.767	1.045	1.397
3	20.708	3.904	1.803	1.612
4	24.937	3.293	1.653	1.426
5	17.647	5.149	3.040	1.781
6	20.325	5.328	2.226	1.459
7	5.145	3.090	1.622	1.105
8	3.628	1.961	0.605	0.347
9	7.241	1.419	1.846	1.426
10	14.295	5.124	4.152	2.286
11	4.258	5.166	3.231	1.592
12	4.496	1.397	0.600	1.000

for the *Truth* and the GRACE and GFO Case 3 estimates and are shown in Fig. 12 and Table 11. The GFO Case 3 mass variation estimates are more accurate than GRACE for six of the eight basins. The annual amplitude and phase errors are given in Table 12. Comparing these results to those presented in Fig. 10 reveals that adding the force model errors to the simulation does degrade the accuracy of the solutions, and narrows the performance gap between the high-altitude accelerometer and low-altitude drag-free missions.

For the Greenland all errors simulation scenario, the average spatial RMS errors are 6.59, 6.59, 5.78, and 5.78 cm of water for the GRACE, and GFO Case 1, 2, and 3 missions respectively. The Greenland measurement noise only scenario showed noticeable differences between GFO Case 2 and GFO Case 3 while this simulation scenario does not, demonstrating that the inclusion of the force model errors limits the effectiveness of the improved ranging precision, even for the low-altitude drag-free scenario. Figure 13 shows the Greenland basin mass variations and the resulting statistics and the trend and annual signal parameters are in Tables 13 and 14 respectively. While GFO Case 3 outperforms GRACE for the majority of basins, the improvements are much smaller than when the force model errors were not included as in Fig. 11. This scenario also shows much larger errors in the estimated trends than was observed for the measurement noise only case, showing that the atmospheric modeling errors have a significant effect on the recovery of the ice mass changes. The degradation in solution accuracy caused by the force model errors is noticeably larger for Greenland than South America because of the larger uncertainties in the atmospheric models.

5 Conclusions

The results of the spatial resolution study (Figs. 8, 9) show that the laser interferometric ranging system provides

Table 9 Truth and estimated Greenland basin trends

Basin	Greenland basin trends (cm/yr)				
	Truth	Meas. noise only		All errors	
		GRACE	GFO 3	GRACE	GFO 3
1	0.13	0.50 ± 0.61	0.24 ± 0.06	0.06 ± 1.73	−0.18 ± 1.31
2	−0.39	−0.39 ± 0.62	0.13 ± 0.18	−0.52 ± 1.68	−0.56 ± 1.08
3	−18.07	−13.84 ± 0.77	−18.89 ± 0.14	−10.50 ± 0.98	−9.47 ± 0.41
4	−27.89	−23.41 ± 0.21	−30.27 ± 0.17	−16.99 ± 1.21	−15.79 ± 0.98
5	−4.96	−3.59 ± 1.57	−2.65 ± 0.25	−8.51 ± 1.35	−6.94 ± 1.35
6	−14.70	−6.83 ± 0.54	−15.66 ± 0.61	−5.04 ± 1.59	−4.35 ± 1.42
7	0.04	1.18 ± 0.50	0.05 ± 0.25	−1.99 ± 1.25	−2.76 ± 1.10
8	0.97	−0.23 ± 0.29	1.14 ± 0.14	−3.10 ± 1.21	−3.80 ± 1.02
9	−7.16	−6.22 ± 0.22	−5.82 ± 0.33	−7.84 ± 1.14	−7.57 ± 0.88
10	−19.58	−13.25 ± 0.87	−15.89 ± 0.18	−13.06 ± 1.23	−12.46 ± 0.97
11	−0.36	−8.59 ± 0.69	−2.91 ± 0.32	−10.51 ± 1.21	−9.95 ± 1.05
12	−2.48	−4.11 ± 0.19	−1.99 ± 0.28	−5.82 ± 1.27	−5.91 ± 1.04

Table 10 Truth and simulated errors (Truth minus estimate) of best fit trend, annual amplitude and annual phase: Greenland measurement errors only (cf. Fig. 11)

Basin	Trend (cm/year)			Annual amplitude (cm)			Annual phase (°)		
	Truth	Truth−Est.		Truth	Truth−Est.		Truth	Truth−Est.	
		GRACE	GFO 3		GRACE	GFO 3		GRACE	GFO 3
1	0.13	−0.37	−0.11	23.88	−2.40	0.76	0.00	−1.84	−0.35
2	−0.39	0.00	−0.52	23.41	−3.15	1.63	0.00	−1.58	0.34
3	−18.07	−4.23	0.82	20.44	−1.93	2.34	0.00	−2.01	0.66
4	−27.89	−4.48	2.38	19.35	0.80	0.40	0.00	4.28	−0.53
5	−4.96	−1.37	−2.31	23.61	0.82	0.82	0.00	1.24	−0.25
6	−14.70	−7.87	0.96	22.24	−0.38	1.43	0.00	−2.30	−1.33
7	0.04	−1.14	−0.01	7.44	3.54	1.26	0.00	6.90	−2.65
8	0.97	1.20	−0.17	5.48	2.54	−0.05	0.00	10.10	−0.92
9	−7.16	−0.94	−1.34	6.47	0.74	0.71	0.00	3.80	−3.43
10	−19.58	−6.33	−3.69	7.12	1.60	0.17	0.00	3.78	−0.10
11	−0.36	8.23	2.55	6.03	1.76	0.41	0.00	2.92	1.45
12	−2.48	1.63	−0.49	5.40	1.41	0.88	0.00	3.52	1.33

significant improvement in recovering the high-resolution features of the static component of the gravity field as compared to the current K-band ranging system for the low-altitude drag-free scenario. These results also show that even in the absence of temporal aliasing, the laser ranging system does not improve the results for a GRACE-altitude mission with on-board accelerometers. The results tabulated in Table 5 show that the limitations imposed by the higher altitude and accelerometers also prevent any improvement with the laser when estimating a more realistic gravity signal, even in the Greenland measurement noise only case which has a large signal and no aliasing errors.

The results of the time-variable gravity simulations (Figs. 10, 11, 12, 13) illustrate some of the challenges associated with understanding the effects of various error sources on the solutions. It has already been discussed that the effects of temporal aliasing are dependent on the way in which the time-varying gravity signal and the geophysical model errors are sampled by the satellite groundtrack. Additionally, the accelerometer errors of GRACE and GFO Case 1 that remain after the estimation of empirical accelerations also manifest themselves differently each month. The unpredictable nature of the spatial and temporal characteristics of the aliasing and accelerometer errors, and the limited number of tracks per

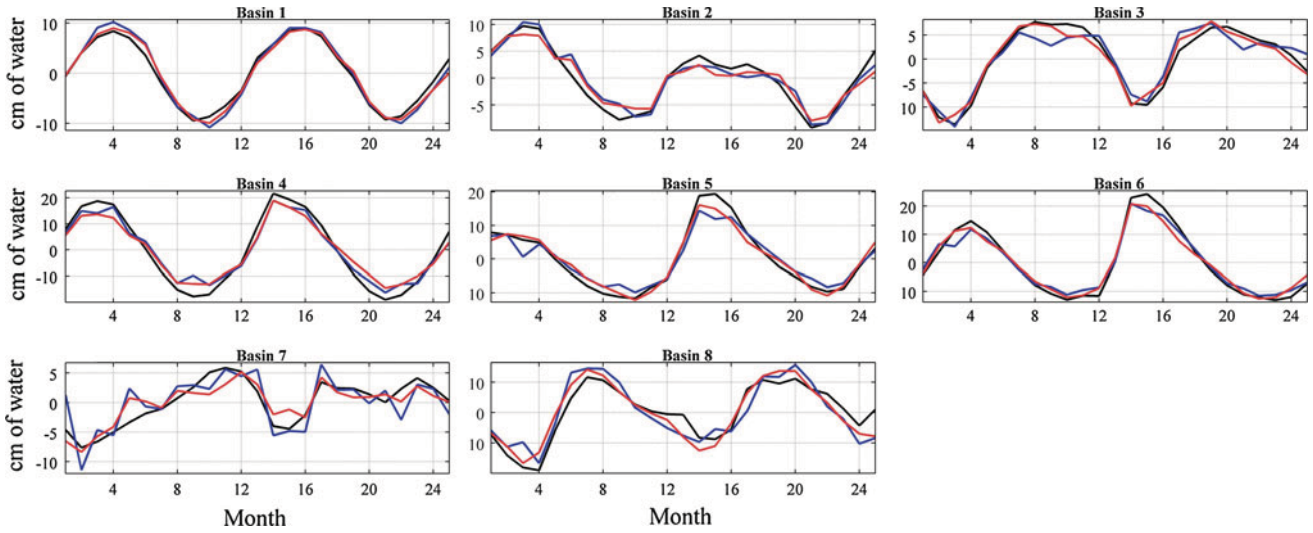

Fig. 12 South America basin mass variations for missions with all error sources: Truth (*black*), GRACE (*blue*), and GFO Case 3 (*red*)

Table 11 Statistical analysis of South American basin mass variations: all errors (cf. Fig. 12)

Basin	Truth RMS (cm of water)	Truth–Estimate RMS (cm of water)	
		GRACE	GFO 3
1	6.222	1.243	1.042
2	5.459	1.617	1.628
3	6.705	2.106	1.267
4	13.609	3.177	3.589
5	9.076	2.587	1.880
6	11.844	2.438	2.310
7	3.790	2.642	1.809
8	8.907	4.546	3.577

month, may produce a situation where these errors effectively cancel each other out over one basin, while they combine to create very large errors over another. This dynamic nature of the errors explains why GFO Case 3 tends to outperform GRACE, but does not in all cases. It also explains why in some cases, the statistical accuracy of a particular basin improves when the geophysical model errors are added to the simulation (e.g. comparing Tables 6 and 11). The time-variable gravity results also show that the accuracy of the basin-scale estimates tend to improve as the size of the basin increases for all simulated mission scenarios. This correlation between basin size and accuracy is primarily due to the fact that these dynamic errors tend to average out over larger basins.

Several conclusions can be drawn from the time-variable gravity results summarized in Table 5. Comparing the results of GFO Case 2 and 3 for the measurement noise only cases demonstrates a lack of improvement from the laser interferometer when hydrological aliasing is considered. The AOD model errors and their aliasing effects also prevent any improvement with the laser as evidenced by comparing the GFO Case 2 and 3 Greenland simulation results with

Table 12 Truth and simulated errors (Truth minus estimate) of best fit annual amplitude and annual phase: South America all errors (cf. Fig. 12)

Basin	Annual amplitude (cm)			Annual phase (°)		
	Truth	Truth−Est.		Truth	Truth−Est.	
		GRACE	GFO 3		GRACE	GFO 3
1	9.21	−0.86	−0.15	10.52	5.84	6.58
2	7.04	1.35	2.02	27.87	8.47	6.22
3	8.40	2.50	0.69	219.58	−8.50	−10.36
4	19.18	4.08	4.67	26.41	3.55	4.00
5	12.48	2.95	1.16	24.33	5.06	2.29
6	15.97	2.73	2.32	2.28	−1.00	−2.44
7	3.24	0.28	1.32	195.61	−8.99	−23.29
8	9.69	−2.61	−2.44	236.32	−9.31	−11.23

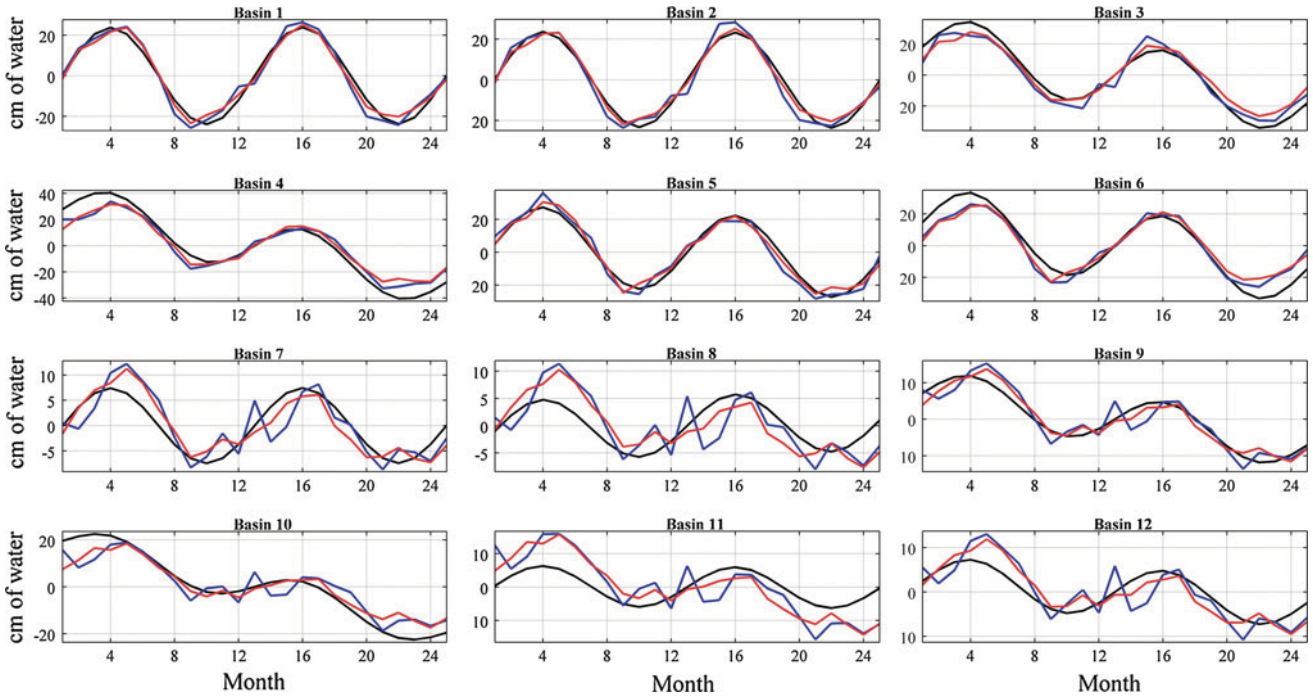

Fig. 13 Greenland basin mass variations for missions with all error sources: Truth (*black*), GRACE (*blue*), and GFO Case 3 (*red*)

Table 13 Statistical analysis of Greenland basin mass variations: all errors (cf. Fig. 13)

Basin	Truth RMS (cm of water)	Truth−Estimate RMS (cm of water)	
		GRACE	GFO 3
1	16.513	3.734	2.707
2	16.306	4.010	2.309
3	20.708	5.464	5.462
4	24.937	7.196	7.814
5	17.647	4.447	3.269
6	20.325	6.663	7.192
7	5.145	3.547	2.619
8	3.628	4.125	3.391
9	7.241	2.979	1.958
10	14.295	5.688	5.062
11	4.258	6.969	6.042
12	4.496	3.865	2.837

and without these errors included. The statistics in Table 5 also reveal that the low-altitude missions consistently have a lower mean spatial RMS error than the high-altitude missions, implying that the drag-free system combined with the lower altitude and smaller spacecraft separation does provide some benefit.

None of the simulations in this study show an improvement in using the laser for the GRACE-altitude accelerometer scenario. This result might initially be surprising due to the difference in range-rate error spectra between GRACE and GFO Case 1 at higher frequencies (see Fig. 3). The similarities in performance between these missions are caused by the long-to-medium wavelength errors that remain after the estimation of empirical parameters which are common to both missions. To recover a coherent gravity signal in the presence of the longer wavelength errors, spatial constraints (or smoothing) must be applied such that the improved mission performance of GFO Case 1 at higher frequencies is largely irrelevant.

This study also illustrates that understanding the effects of geophysical signals and their errors on mission performance requires analyzing a time-series of simulated data, rather than just a single snap-shot. Additionally, the accuracy of regional gravity estimates can vary significantly based on location due to the geographic dependence of the geophysical model errors and the strength and temporal variability of the hydrological signal. Due to the spatial and temporal variations in errors, a global description of errors at a single point-in-time (e.g. a degree-variance plot of errors), is not necessarily a good representation of mission performance.

In summary, to realize the full benefit of a laser interferometer would require that it be accompanied by a reduction in both the accelerometer errors and the temporal aliasing errors from what was assumed in this study. The accelerometer errors could possibly be reduced by improving the data processing methods (e.g. improved parameterization of the accelerometer data), or by flying a GFO mission equipped with a drag-free system. Reducing the

Table 14 Truth and simulated errors (Truth minus estimate) of best fit trend, annual amplitude and annual phase: Greenland all errors (cf. Fig. 13)

Basin	Trend (cm/year)			Annual amplitude (cm)			Annual phase (°)		
	Truth	Truth−Est.		Truth	Truth−Est.		Truth	Truth−Est.	
		GRACE	GFO 3		GRACE	GFO 3		GRACE	GFO 3
1	0.13	0.07	0.31	23.88	−0.73	1.50	0.00	−4.42	−1.19
2	−0.39	0.13	0.17	23.41	−1.19	1.07	0.00	−4.70	−1.25
3	−18.07	−7.57	−8.60	20.44	−2.01	0.36	0.00	−3.20	−0.15
4	−27.89	−10.90	−12.10	19.35	−0.04	0.71	0.00	1.59	2.72
5	−4.96	3.55	1.98	23.61	−0.15	1.27	0.00	−5.30	−1.06
6	−14.70	−9.66	−10.35	22.24	−0.26	1.48	0.00	−4.94	−1.06
7	0.04	2.03	2.80	7.44	0.95	1.30	0.00	15.48	11.20
8	0.97	4.07	4.77	5.48	0.76	1.07	0.00	23.32	17.66
9	−7.16	0.68	0.41	6.47	0.36	0.71	0.00	10.95	12.04
10	−19.58	−6.52	−7.12	7.12	0.69	0.58	0.00	16.14	13.98
11	−0.36	10.15	9.59	6.03	0.79	0.68	0.00	16.44	15.61
12	−2.48	3.34	3.43	5.40	0.72	0.93	0.00	16.86	16.31

aliasing errors is a greater challenge in that it cannot simply be solved through improved instrumentation. It is conceivable that sophisticated methods of data processing, such as a technique that analyzes the data along-track, might effectively improve the temporal resolution of the solutions, thus reducing this error. Additionally, alternative architectures for a follow-on mission might be investigated to determine if different mission configurations, such as a constellation of satellites, would reduce the aliasing errors. Lastly, any improvements in the geophysical models would reduce the aliasing errors, and thus a GFO with upgraded technologies would provide greater benefits than were observed in this study.

Acknowledgments This work was supported by NASA Headquarters under the Earth System Science Fellowship Grant NGT5 and the NASA Instrument Incubator Program (IIP) through ESTO at NASA/GSFC.

References

Bender PL, Nerem RS, Wahr JM (2003) Possible future use of laser gravity gradiometers. Space Sci Rev 108:385–392

Bertiger W, Bar-Sever Y, Bettadpur B, Desai S, Dunn C, Haines B, Kru- izinga G, Kuna D, Nandi S, Romans L, Watkins M, Wu S (2002) GRACE millimeters and microns in orbit. In: Proceedings of ION GPS 2002, Portland

Carrère L, Lyard F (2003) Modeling the barotropic response of the global ocean to atmospheric wind and pressure forcing—comparison with observations. Geophys Res Lett 30(6):1275–1278. doi:10.1029/2002G016473

Dehne M, Cervantes FG, Sheard B, Heinzel G, Danzmann K (2009) Laser interferometer for spaceborne mapping of the Earth's gravity field. J Phys Conf Ser **154**. doi:10.1008/1742-6596/154/1/012023

Flechtner F (2007) AOD1B product description document for product releases 01 to 04, GRACE 327-750 (GR-GFZ-AOD-0001)

Flury J, Rummel R (2006) Future satellite gravimetry and Earth dynamics. In: Flury J, Rummel R (eds) Earth, Moon, and Planets, vol 94. Nr. 1, Springer, ISBN (Print) 978-0387-29796-5. doi:10.1007/0-387-33185-9

Han S-C, Jekeli C, Shum CK (2004) Time-variable aliasing effects of ocean tides, atmosphere, and continental water mass on monthly mean GRACE gravity field. J Geophys Res 109:B04403. doi:10.1029/2003JB002501

Kang Z, Tapley B, Bettadpur S, Ries J, Nagel P (2006) Precise orbit determination for grace using accelerometer data. Adv Space Res 38:2131–2136

Kim J-R (2000) Simulation study of a low-low satellite-to-satellite tracking mission, Ph.D. thesis, University of Texas, Austin

Lefèvre F, Lyard F, LeProvost C, Schrama E (2002) FES99: a global tide finite element solution assimilating tide gauge and altimetric information. J Atmos Ocean Technol 19:1345–1356

Luthcke SB, Arendt AA, Rowlands DD, McCarthy JJ, Larsen CF (2008) Recent glacier mass changes in the Gulf of Alaska region from GRACE mascon solutions. J Glaciol 54(188):767–777

Luthcke SB, Rowlands DD, Lemoine FG, Klosko SM, Chinn D, McCarthy JJ (2006) Monthly spherical harmonic gravity field solutions determined from GRACE inter-satellite range-rage data alone. Geophys Res Lett 33:L02402. doi:10.1029/2005GL024846

Marchetti P, Blandino JJ, Demetriou MA (2008) Electric propulsion and controller design for drag-free spacecraft operation. J Spacecraft Rockets 45(6):1303–1315. doi:10.2514/1.36307

Nerem RS, Bender P, Loomis B, Watkins MM, Folkner WM, Stephens M, Craig R, Leitch J, Pierce R (2006) Development of an interferometric laser ranging system for a follow-on gravity mission to GRACE. Eos Trans AGU **87**(52), Fall Meet. Suppl. Abstract G11B-02

Pierce R, Leitch J, Stephens M, Bender P, Nerem RS (2008) Inter-satellite range monitoring using optical interferometry. Appl Opt 47(27):5007–5018

Ray RD (1999) A global ocean tide model from TOPEX/POSEIDON altimetry: GOT99, NASA technical memorandum 209478, Goddard Space Flight Center

Rodell M, Houser PR, Jambor U, Gottschalck J, Mitchell K, Meng C-J, Arsenault K, Cosgrove B, Radakovich J, Bosilovich M, Entin JK, Walker JP, Lohmann D, Toll D (2004) The global land data assimilation system. Bull Am Meteorol Soc 85:381–394

Rowlands DD, Luthcke SB, McCarthy JJ, Klosko SM, Chinn DS, Lemoine FG, Boy J-P, Sabaka T (2010) Global mass flux solutions from GRACE; a comparison of parameter estimation strategies: mass concentrations versus Stokes coefficients. J Geophys Res 115:B01403. doi:10.1029/2009JB006546

Rummel R (2003) How to climb the gravity wall. Space Sci Rev **108**, 1–14. doi:10.1023/A:1026206308590

Seo KW, Wilson CR, Chen J, Waliser DE (2008) GRACE's spatial aliasing error. Geophys J Int 172:41–48. doi:10.1111/j.1365-246X.2007.03611.x

Seo KW, Wilson CR (2005) Estimating GRACE aliasing errors. Int Assoc Geod Symp 129:339–345. doi:10.1007/b138327

Sneeuw N, Flury J, Rummel R (2005) Science requirements on future missions and simulated mission scenarios. Earth Moon Planets 94(1):113–142. doi:10.1007/s11038-004-7605-x

Swenson S, Wahr J (2002) Methods for inferring regional surface-mass anomalies from Gravity Recovery and Climate Experiment (GRACE) measurements of time-variable gravity. J Geophys Res 107(B9):2193. doi:10.1029/2001JB000576

Tapley BD, Bettadpur S, Watkins M, Reigber C (2004) The gravity recovery and climate experiment: mission overview and early results. Geophys Res Lett 31:L24806. doi:10.1029/2004GL021220

Tapley B, Ries J, Bettadpur S, Chambers D, Cheng M, Condi F, Gunter B, Kang Z, Nagel P, Pastor R, Pekker T, Poole S, Wang F (2005) GGM02—An improved earth gravity field model from GRACE. J Geod. doi:10.1007/s00190-005-0480-z

Thompson PF, Bettadpur SV, Tapley BD (2004) Impact of short period, non-tidal, temporal mass variability on GRACE gravity estimates. Geophys Res Lett 31:L06619. doi:10.1029/2003GL019285

van Dam T, Visser P, Sneeuw N, Losch M, Gruber T, Bamber J, Bierkens M, King M, Smit M (2008) Monitoring and modeling individual sources of mass distribution and transport in the Earth system by means of satellites. Final Report, ESA Contract No. 20403

Wahr J, Swenson S, Zlotnicki V, Velicogna I (2004) Time-variable gravity from GRACE: first results. Geophys Res Lett 31:L11501. doi:10.1029/2004GL019779

Wiese D N, Folkner W M, Nerem R S (2008) Alternative mission architecture for a gravity recovery satellite mission. J Geod. doi:10.1007/s00190-008-0274-1

Wunsch C, Stammer D (1997) Atmospherical loading and the oceanic 'inverted barometer' effect. Rev Geophys 35(1):79–107